Journal of Materials Chemistry A

Accepted Manuscript

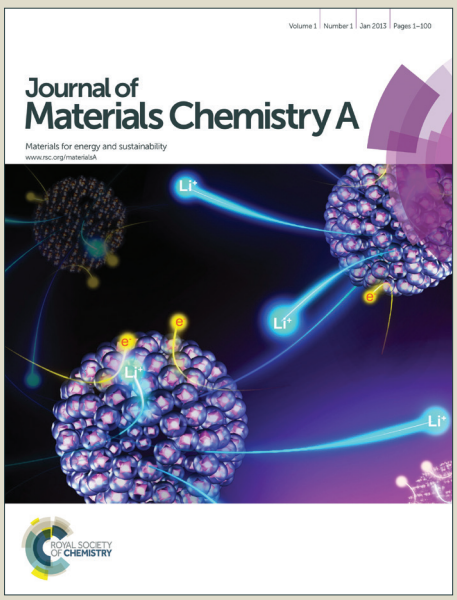

ROYAL SOCIETY OF CHEMISTRY

www.rsc.org/materialsA

Reactive Adsorption of CEES on Iron Oxyhydroxide/(N-)Graphite Oxide Composites under Visible Light Exposure

Javier A. Arcibar-Orozco[a], Silvio Panettieri[a, b,] and Teresa J. Bandosz[a, b]*

[a] Department of Chemistry, The City College of New York, New York, NY 10031, USA.

[b] The Graduate Center of the City University of New York, 365 Fifth Avenue, New York, NY, 10016, USA.

* E-mail: tbandosz@ccny.cuny.edu; Fax: +1-212-650-6107; Tel: +1-212-650-6017

Table of Content Entry

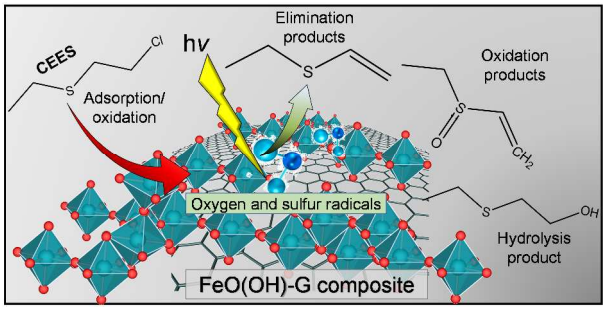

The addition of graphite oxide and aminated graphite oxide increases the oxidative potential of iron oxyhydroxides leading to the efficient adsorption, oxidation, and elimination of chloroethyl ethyl sulfide.

Abstract

The interactions of 2-Chloroethyl ethyl sulfide (CEES) with the surface of iron oxyhydroxide and its composite with graphite oxide and/or aminated graphite oxide were studied under a visible light irradiation. Materials exposed to CEES were extensively characterized by FTIR-STR, UV-VIS-NIR, and TA-MS. The gaseous/vaporous reaction products were identified by GC-MS. The compounds deposited on the surface of the materials were analyzed in acetonitrile extracts by NMR and MS-MS. The FTIR results indicated the existence of alcohol groups on the surface of the exhausted samples, and the involvement of OH groups in the CEES reactive adsorption. Ethyl vinyl sulfide (EVS) was the only volatile compound detected as a result of the reaction with the surface. Two adsorption sites for either CEES or EVS were identified on the adsorbents ´surface. As a result of CEES reactive adsorption Fe(III) was reduced which indicates its crucial role in oxidation of CEES and EVS. On the composites, the detection of a product of advanced oxidation of CEES, disulfides, suggests the activation of thiyl and oxygen radicals. This indicates that the incorporation of GO and GOU into iron oxyhydroxides strongly increases the oxidation potential of oxyhydroxides and induces the formation of radicals. The main promoters of CEES transformation are proposed to be OH groups and thiyl radicals.

Keywords

Iron, Inorganic composites, 2-Chloroethyl ethyl sulfide, mustard gas surrogate, reactive adsorption

Introduction

The interest in the study of destruction of chemical warfare agents (CWA) has re-garnered attention in recent years, due to the increase in the probability of these compounds usage in

chemical wars or terrorist attacks. 2-Chloroethyl ethyl sulfide (CEES) is a surrogate of the chemical warfare sulfur mustard: bis(2-Chloeroethyl sulfide).[1] Studies on its detoxification mechanisms can bring a significant input to the comprehending the actual chemical warfare agent detoxification. Understanding the principles of the chemical interactions and the degradation pathways are key factors in creating multifunctional materials capable to efficiently destroy CWA. The latter can be spread during malicious attacks either in drinking water or in the vapor forms. It has been reported that both liquid CEES and its vapors can be removed by means of adsorption/photocatalysis approaches. Highlighted removal materials are: brominated polymers[2], Metal Organic Frameworks (MOFs)[1] Zeolites,[3] TiO_2,[4-6] MgO,[7] Al_2O_3,[7, 8], V_2O_5,[9] and several metal oxides-based catalysts. [10, 11] Most of the studies that described the degradation pathway of CEES focused on TiO_2 and its activity under UV-radiation.

Voronstov and co-workers[4] reported that the gaseous products of CEES photocatalysis on TiO_2 are formed following an oxidation pathway. The surface reactions of CEES led to various products. Two main compounds were 2-chloroethyl ethyl sulfoxide and bis(2-chloroethyl) disulfide. It was reported that the photocatalytic oxidation of sulfides was triggered by radical reactions and by the further reaction of CEES with oxygen (or superoxide ions) to form sulfones and sulfoxides. Besides oxidation, the proton elimination assists in the formation of ethylene and chloroethylene that were detected in the gas phase of the photocatalytic oxidation reactors. Nevertheless, most of CEES remained unchanged and adsorbed on the surface of the materials, which contributed to a TiO_2 exhaustion. On the other hand, Martyanov and Klabunde[5] reported that the main CEES elimination pathway is a direct attachment of a photogenerated hole that leads to the formation of a thioether cation, which yields sulfoxide. The prevalence of the oxidation mechanism over hydrolysis was also reported in V_2O_5 nanotubes.[9] There the formation

of CEES oxidation products was explained by the reaction of sulfur and the metal ion at the lattice point (terminal oxygen) leading to the formation of CEES sulfoxides.

Therefore, in the search of efficient materials for CEES elimination it is interesting to study oxidizing semiconductors, in order to promote the oxidation over the hydrolysis pathway. In this matter it's essential that the materials also have a high surface area with available reactive adsorption centers for the oxidation of CEES.

Iron oxyhydroxides are versatile materials that are known as excellent oxidizing agents.[12] They have tunable features and excellent catalytic properties. They can be photoactive, having a band gap that can be located in the visible range, depending on the synthesis conditions and on the crystal structure of the specific iron oxyhydroxide.[13-17] Moreover, due to their porosity and a relatively high surface area, they have been proven to be excellent adsorbents from the vapor/gas phase. In addition, they can be rapidly and easily produced on industrial scales, using a low cost synthesis process.

Even though the degradation of mustard gas with goethite-zirconia[18] and goethite-titania[19] were reported previously, the products of surface reaction were not analyzed in details. In our previous study[20] we reported the formation of iron oxyhydroxide/graphite oxide and iron oxyhydroxide/aminated graphite composites and their applications for the removal of CEES vapors. The composites consisted mainly of the high surface area 2-line ferrihydrite with a small fraction of akageneite, with an optical band gap in the visible range. The materials were efficient in removing CEES vapors and a correlation between the amount adsorbed and the porosity was reported.

The objective of the present study is to determine/analyze interactions between CEES and the surface of iron oxyhydroxide (FeOH), and the iron oxyhydroxide/GO (FeOH-GO), andiron oxyhydroxide/GO-N composites (FeOH-GOU). A detailed characterization of the materials exposed to CEES in visible light was carried out (The materials exposed to CEES are referred with an addition letter "E"). Volatile and surface reaction products were analyzed by spectroscopic techniques and based on the reaction products, the mechanisms of adsorption/oxidation/hydrolysis that occur on the surface of the materials were proposed. The emphasis is on the effects of the visible light on the surface reactivity/decontamination extent.

Results and discussion

The FTIR-ATR spectra of the samples before and after CEES exposure are presented in Fig. 1. After CEES exposure, all samples show the appearance of the same new bands but with various intensities. The most obvious features are seen for FeOH and thus, as an example, the assignment of the bands are carried out on this material. The band at 3390 cm^{-1} is linked to an OH stretching of bulk groups in iron hydroxide[21] and also to adsorbed water in the samples. The band at around 1650 cm^{-1} represents the bending of OH groups in water. After CEES exposure, there is a widening of this band which can be the result of the stretching of the O-H bond in alcohol groups. [22] The band at 1419 cm^{-1} can be attributed to the deformation of a CH_2OH group ($\nu S(COO-)$), whereas the band at 1267 cm^{-1} can be due to a C-O stretching in CH_2OH. These bands, along with the widening of the O-H band, are the first indication of alcohols formation as a result of the reaction of the OH groups of the iron hydroxide phase with CEES.

Other bands that can be linked to CEES are the twin bands at 2973 and 2923 cm^{-1} that are assigned to C-H stretching vibrations.[22] A band at 1450 cm^{-1} is attributed to C-H asymmetric vibrations of CH_2 and CH_3 groups and a band at 1375 cm^{-1} corresponds to symmetric deformations of C-H on CH_3. Finally, a band at 1045 cm^{-1} originates from vibrations of the R-SO_3-, and also R_2SO, indicating the presence of compounds with oxidized sulfur as a result of CEES reactive adsorption. On the spectra for the GO and GOU composites after CEES exposure, the bands are less pronounced. However, there is clear evidence of bands at 3400, 2969, 1454, 1386, 1270, and 1047 cm^{-1}. The assignments of these bands are the same as for FeOH. On the spectra for the exhausted FeOH and FeOH-GOU there are bands at 1627 and 1616 cm^{-1}, which corresponds to the iron-oxygen bond vibration. For FeOH-GO this band is not present, therefore suggesting the involvement of Fe-O (oxygen bridges) in the CEES reactive adsorption.

The simultaneous thermal analysis-mass spectrometry (TA-MS) was carried out in order to determine the nature of the CEES interactions and/or its decomposition products. The derivative weight loss and the MS thermal profiles are shown in Figures 2-4. Peaks on the DTG curves are numbered in order to facilitate their identification using the MS results.

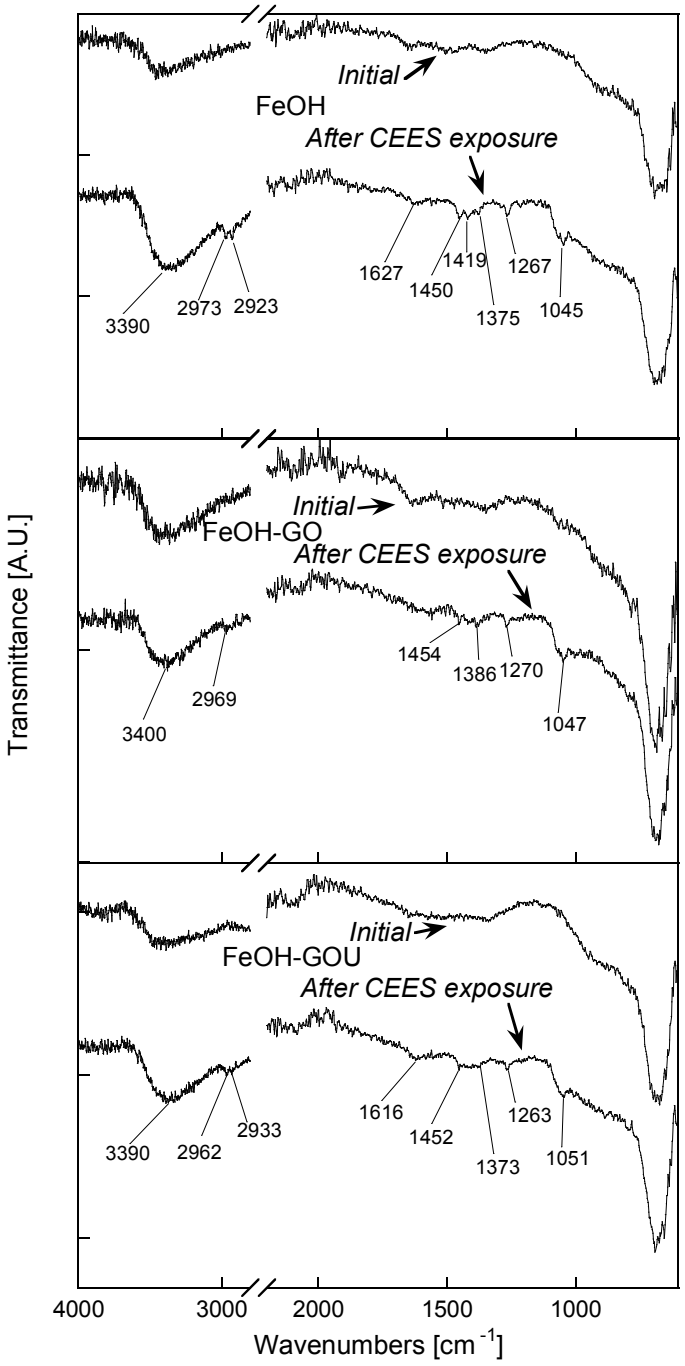

Figure 1. FTIR spectra of the samples studied before and after exposure to CEES.

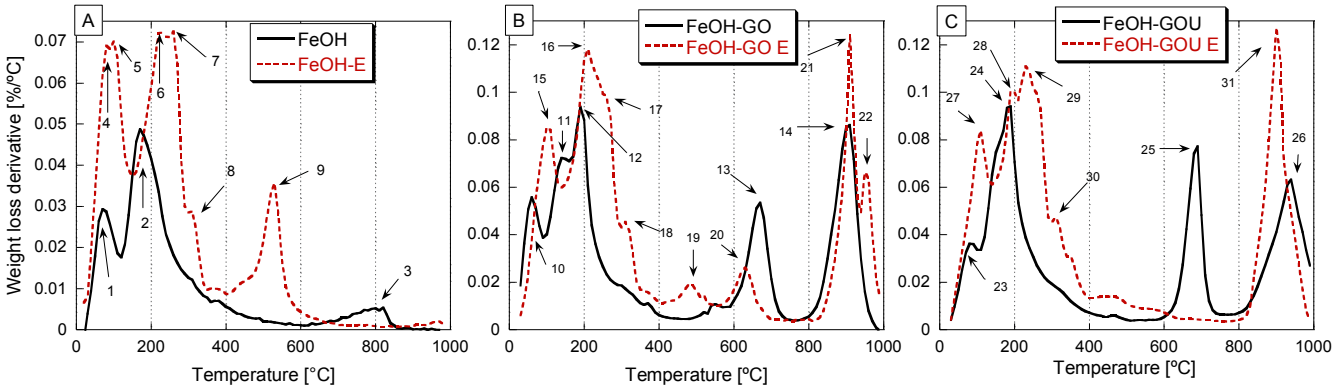

Figure 2. DTG curves in helium for FeOH (A), FeOH-GO (B), and FeOH-GOU (C) before and after CEES exposure.

Before CEES exposure, the DTG curve of the FeOH sample (Figure 2A) showed 2 main peaks at 70 and 170 °C, and a small peak at around 810 °C. They can be assigned to: 1) dehydration of the iron hydroxide, 2) dehydroxylation of $Fe(OH)_3$ that lead into the formation of Fe_2O_3, and 3) the minor reduction of Fe(III). After CEES exposure, there is the appearance of several new peaks on the DTG curves. The assignment is based on detected m/z fragments (Figures 3 and 4). Peaks 4 and 5 are closely related as they have maximums at temperatures of 77 and 100 °C. This indicates that two compounds that have similar decomposition/boiling temperatures are released from the material's surfaces. Around the temperature of peak 4, the MS spectra displayed strong signals at m/z 75 (CH_3-CH_2-S^+-CH_2), 62 (CH_3-CH_2-S^+H), 61 (CH_3-CH_2-S^+), 47 (CH_2=S^+H), and 27 ($C_2{}^+H_3$), (Figure 3A) that are important fragments of CEES.[23, 24] Around the temperature of peak 5, the signals of CEES were still detected and also m/z signals of 88, 73, 60, and 59 (Figure 3B). These signals are related to another compound than CEES that desorbs from the surface. Considering the mass spectra and the volatilization temperature, it is likely that this compound is ethyl vinyl sulfide (EVS), whose fragmentation of CH_3-CH_2-S-CH_2=C^+H, and its series differs from that of CEES. Therefore, both peaks 4 and 5 are likely related to the removal of CEES and

EVS. Even though CEES has a boiling point of 156 °C [25] and EVS of 97 °C,[25] the peak of CEES is located at a temperature slightly lower than the one of EVS. This can indicate that the interaction energies of EVS are stronger than those of CEES, therefore delaying its thermal desorption. Peaks 6 and 7 correspond also to CEES and EVS respectively, and peak 8 represents CEES. The existence of two desorption temperatures of the same compound (either CEES or EVS) indicates two energetic sites in which this compound is adsorbed on the surface. The first peak represents the removal of weakly adsorbed molecules that are probably deposited in large pores and/or on the external surface. On the other hand, the sites related to the second decomposition temperature represent high adsorption energy and therefore they are likely located in the small pores. At the temperature of the second peak the presence of H_2S, and SO_2 was also detected. They are formed in the reaction of the CEES and/or EVS with oxygen and hydrogen released from the surface of the materials during the iron dehydroxylation. Finally, peak 9 corresponds to the reduction of Fe(III) that is accompanied by carbon oxidation.[26]

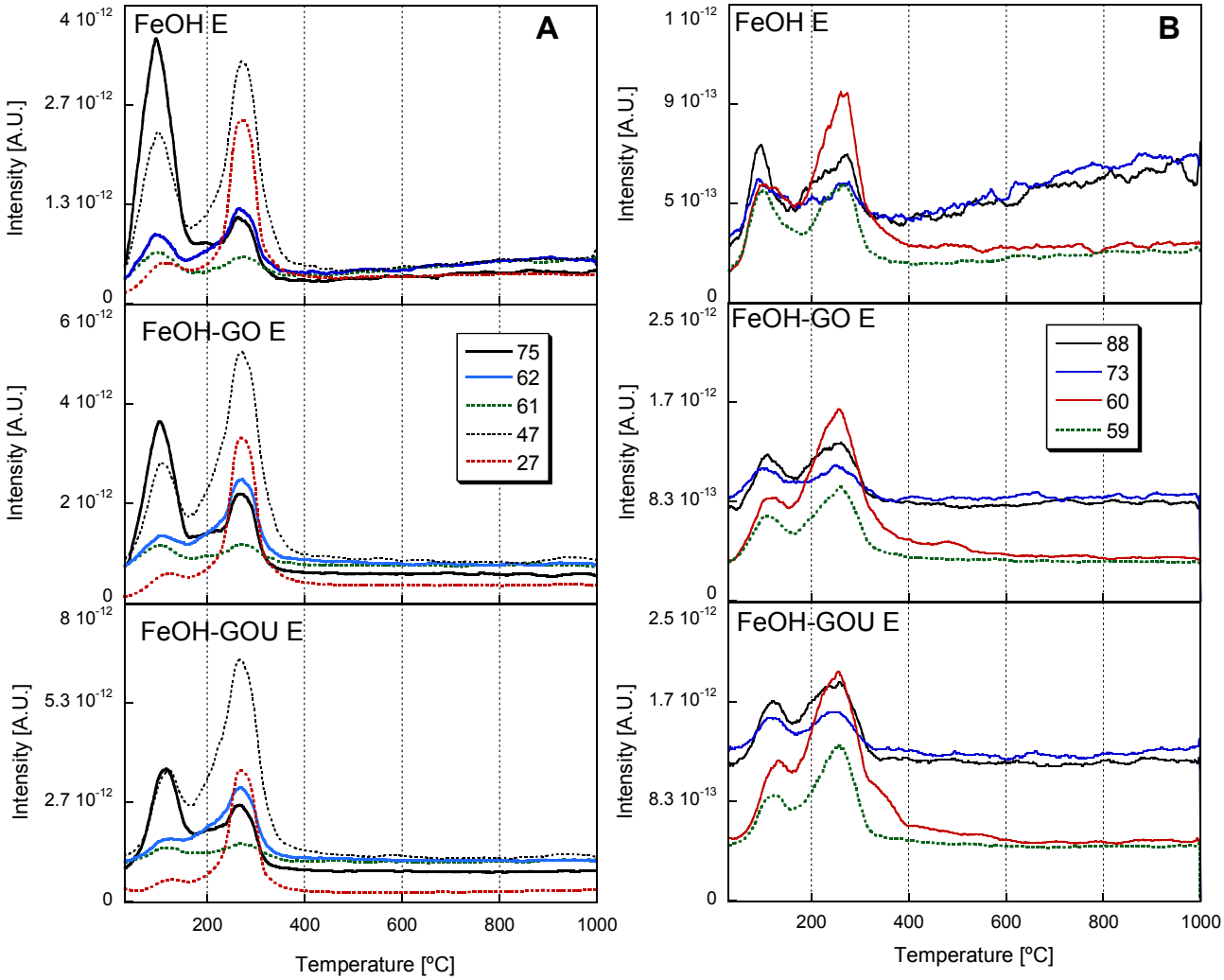

Figure 3. Mass to charge (m/z) thermal profiles used for the identification of CEES A) and EVS B). The multiplication factors are: 27(x0.1), 47(x5), 59(x2), 60(x2), 61(x5), 62(x5), 73(x5), 75(x4), and 88(x5).

The evolution of the m/z signals corresponding to the sulfur fragments also provides valuable information about the nature of the compounds desorbed from the surfaces (Figure 4). At around 250 °C the signals of m/z 64 and 66 (SO_2) are intense. They likely represent the oxidation of CEES and/or EVS when desorbing from the surface. However, at this temperature the concentration of oxygen should be low (see m/z 32 in Figure 4) and the dehydration of the surface should be its only source. Therefore, it is plausible to assume that the SO_2 signal is

coming from the decomposition of an oxidized compound, produced on the surface of FeOH. These signals disappeared around 350 °C and appeared again at 530 °C, which corresponds to peak 9. This peak was not accompanied by any signal related to CEES or EVS. However, at this temperature a low intensity signal of m/z 44 (CO_2 in Figure 4) was detected. Therefore, this peak represents the combustion of a compound that was formed on the surface of FeOH that decomposes into CO_2 and SO_2. This is probably an oxidized product of the CEES reactive adsorption that was strongly adsorbed or chemisorbed on the FeOH sample.

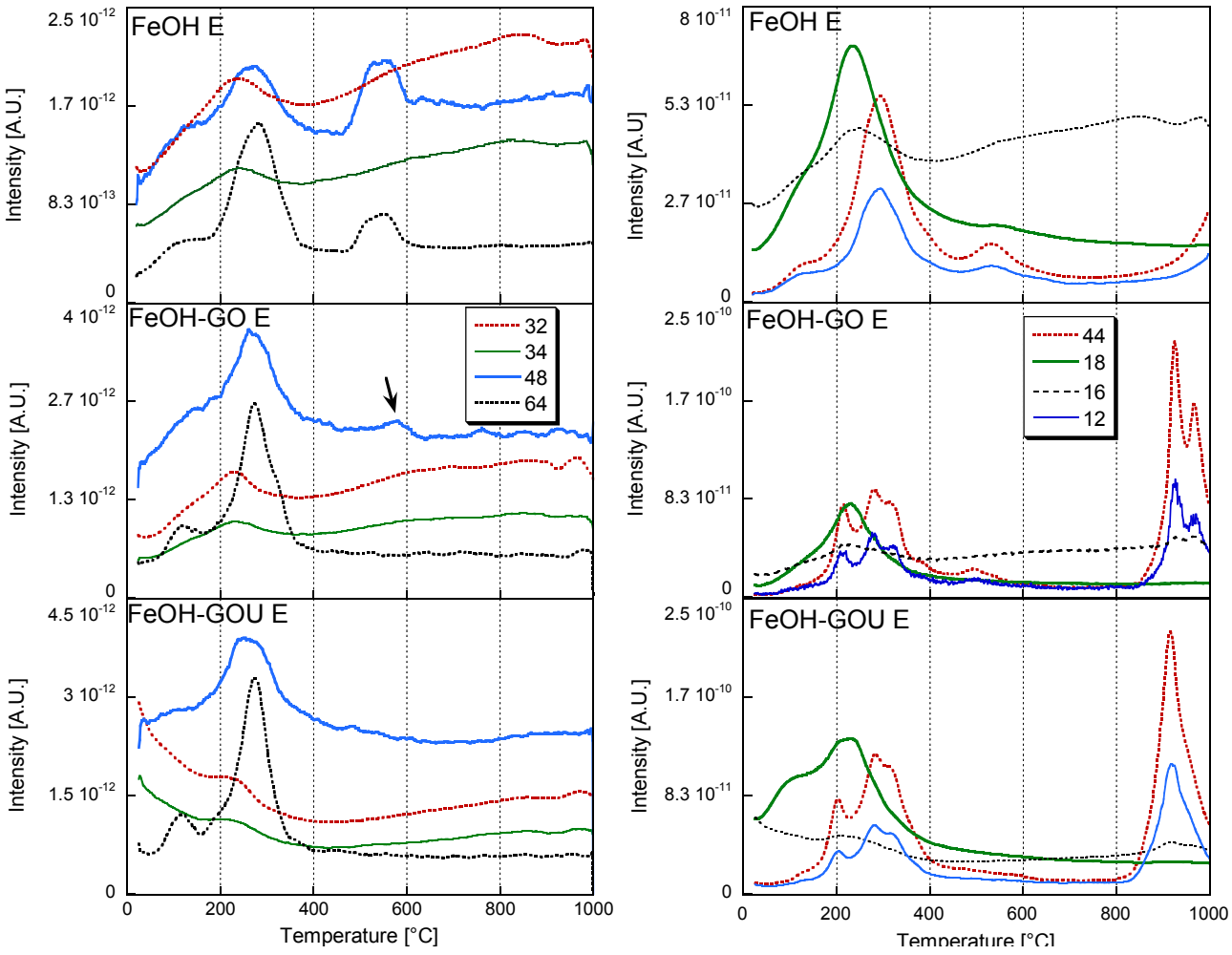

Figure 4. m/z thermal profiles of SO_2 (64(x1.5), and 48 (x7)), SO (34(x0.3) and 32(x0.002)), O_2 (m/z 32), water (18x, and 16x), and CO_2 (44x and 12x).

The DTG curve of FeOH-GO (Figure 2B) shows a different pattern than that of FeOH. The curve for the initial sample reveals 5 peaks (peaks 10-14), located at 60, 140, 186, 670, and 908 °C. Peak 10 represents the evaporation of adsorbed water, peak 11 corresponds to the decomposition of the remaining epoxy groups of GO.[27] Peaks 12-14 are due to the dehydroxylation of the iron phase, the reduction of iron (III) to iron (II), and to the reduction of iron (II) to iron (0) promoted for the presence of the carbon phase, respectively.[28] After CEES exposure 8 peaks (peaks 15-22) were detected. Peak 15 at 105 °C is related to the removal of EVS and CEES, similar to that described for FeOH. It is interesting to note that the peak attributed to the decomposition of epoxy groups in the initial sample (peak 11) was not found on the DTG curves for the exhausted sample. This result suggests the involvement of these groups during the CEES reactive adsorption. At 208 °C, peak 16 corresponds to the decomposition of EVS. The detection of EVS continues until 400 °C and is seen as peaks 17 and 18. On the other hand, CEES signals are more pronounced around 300 °C (peak 18). It is worth mentioning that the peak detected on the DTG curve for FeOH at 530 °C, corresponding to SO_2, is still present on the DTG curve for the exhausted sample, however its intensity is very small (see the arrow in Figure 4).

The DTG curve for FeOH-GOU (Figure 2C) has a similar trend to that for FeOH-GO, however, no evidence of remaining carboxylic groups was found. This is due to the coordination of these groups with amine groups during the treatment of the graphite oxide with urea.[29] Peaks 23-26 are located at 80, 186, 690, and 937 °C, respectively. After CEES exposure, peak 27 at 108 °C corresponds to CEES and EVS, and peak 28 at 190 °C to EVS. Peak 29 at 236 °C represents EVS, while the peak 30 at 310 °C can be linked to both CEES and EVS. It is of particular interest for this sample that the peak at 500 °C, observed for FeOH and FeOH-GO after CEES

exposure, was not detected. Also the peak at 700 °C (peak 25), previously attributed to the iron(III) reduction in the initial sample, was not observed on the DTG curves of the samples after CEES exposure. This is an evidence of the FeOH-GOU's surface reduction during the CEES reactive adsorption.

The comparison of the relative intensities of the m/z fragments representing CEES provides information about distribution of the strength of CEES adsorption energy. The intensity of the first CEES peak for FeOH is markedly higher than that of the second one. The opposite is observed for the composites, for which the intensity of the CEES second peak exceeds the first one. The highest intensity of the second peak is found for exhausted FeOH-GOU. These results indicate that the uptake of CEES is more energetically favorable on the composites with GO and GOU than on iron oxyhydroxide itself. The intensity of the peaks on the m/z thermal profiles differ for the exhausted samples, and the highest signal is found for FeOH-GOU. This is due to the high adsorption capacity on this sample as reported previously.[20] Table 1 summarizes the weight losses represented by the peaks on DTG curves along with their assignments to the specific processes/compounds.

Table 1. Percentage of weight loss and the assignment of the specific peak on the DTG curves for the initial samples and those exposed to CEES vapors.

Peak	% of weight loss	Assignment
FeOH		
1	2.1	Dehydration of iron hydroxide
2	11	Dehydroxylation of the $Fe(OH)_3$
3	4.3	Reduction of iron(III) to iron (II)
FeOH E		
4	5.6	CEES
5	5.6	EVS
6	8	CEES
7	2.8	EVS
8	1.5	EVS/Oxidized sulfur compound
9	8.7	Oxidized sulfur compound
FeOH-GO		
10	2.7	Dehydration of iron hydroxide
11	4.1	Decomposition of GO remaining epoxy groups
12	6.5	Dehydroxylation of the $Fe(OH)_3$
13	4.0	Iron(III) reduction to iron(II)
14	6.9	Iron(II) reduction of iron(0)
FeOH-GO E		
15	6.1	CEES and EVS
16	10.1	EVS
17	3.6	EVS
18	1.7	EVS and CEES
19	1.3	Oxidized sulfur compound
20	2.1	Iron(III) reduction to iron(II)
21	5.5	Iron(II) reduction to iron(0)
22	2.2	Iron(II) reduction to iron(0)
FeOH-GOU		
23	2.1	Dehydration of iron hydroxide
24	11	Dehydroxylation of the $Fe(OH)_3$
25	4.3	Iron(III) reduction to iron(II)
26	6.7	Iron(II) reduction to iron(0)
FeOH-GOU E		
27	5.6	CEES and EVS
28	5.6	EVS
29	8	EVS
30	2.8	EVS and CEES
31	8.7	Iron (II) reduction to iron (0)

The UV-VIS-NIR spectra of the compounds before and after CEES exposure provide information about the changes in the electronic transitions in the materials. The spectra are shown in Figure 5. The absorption bands in the samples originate from the electronic transitions of the $3d^5$ shell of the iron(III) ion. The spectrum for the initial FeOH shows a maximum of reflectivity around 750 nm and a maximum absorption at about 479 nm. This band corresponds to the electron pair transition: $(2(^6A_1)\rightarrow 2(^4T_1))$,[30] that has a large influence on the color of the metal hydroxides. The same electron pair transition (EPT) is found for FeOH-GO and FeOH-GOU at 475 nm. This small shift in the transition might be due to the introduction of GO (black body) into the materials and the formation of Fe-O-C bond.[31]

After exposure to CEES two interesting effects are observed: 1) A shift in the maximum absorption band to the red (to 510 nm in the FeOH and to 493 nm in the composites). This shift can be due to the presence of the interactions of iron(III) with the adsorbed organic molecules, therefore affecting the energy of the EPT band; 2) The appearance of a reflectance band after the maximum absorption band has been reached (below 470 nm). The reflectance band is observed around 370 nm in the exhausted materials. The maximum absorption peak of CEES is at about 210 nm[5] and it has zero light absorption at any other wavelength. Therefore, this band cannot be explained by the presence of the adsorbed CEES molecules, but by a change in the iron(III) transitions. On ferrihydrite around that wavelength the $^6A_1\rightarrow {}^4E_1{:}^4A_1$ ligand field transition (LFT) has been reported.[32] This transition in principle is spin and parity forbidden. However, the magnetic couple of neighboring Fe(III) allows the transition. Any change in the electronic distribution of the iron octahedra, caused by the formation of bonds, might have an effect in the LFT transitions. If the LFT transition becomes forbidden again, the reflectance of the material in

that particular wavelength will increase. This suggests the involvement of the d electrons of the Fe(III) ion in the CEES reactive adsorption and/or its degradation products.

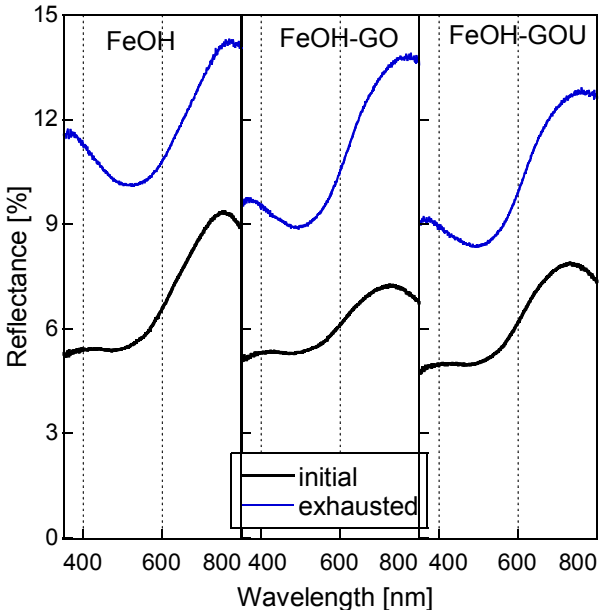

Figure 5. UV-VIS-NIR diffuse reflectance spectra of the samples before and after exposure to CEES

The only gaseous product identified in the headspace was EVS (Spectra shown in Figure S1 in Supplementary Information), indicating that once produced EVS can remain on the adsorbent surface, and/or be volatilized, and/or be further transformed. EVS has been identified as an intermediate of the CEES mineralization on materials such as, TiO_2,[4] $Zn(OH)_2$,[33] and cement .[34] Other studies have reported that in the presence of water EVS was not formed.[3] This is probably due to the formation of hydroxyl species after the fast hydrolysis of Cl^-. Is important to mention that on the blank experiments (light irradiation without the material) the only product on the headspace was CEES, discarding CEES photolysis caused by visible light irradiation.

In order to qualitatively and semi-quantitatively determine the products of the CEES reactive adsorption, extraction of the surface species with acetonitrile was carried out. The extracts were analyzed by NMR and MS-MS, for which deuterated and regular acetonitrile were employed, respectively.

The results of the NMR analysis are shown in Figure 6 along with the peak assignment. The spectrum of FeOH shows triplets at 3.7, 2.8, and 1.2 ppm, and a quadruplet at 2.6 ppm that match with the CEES standard. The EVS was identified via the characteristic peaks located in the olefinic region (5-6.5 ppm) showing the terminal protons between 5.1 and 5.2 ppm as doublets and the internal proton at 6.4 ppm as a double doublet. A third compound having a similar peak pattern to that of CEES was also detected but none of the standards available showed a proper match in terms of chemical shifts. Therefore, we resorted to artificially subtracting the peaks assigned to CEES to yield a cleaner spectrum. Figure 6 shows that this resulted in the generation of a triplet at 1.2 ppm, a double doublet at 2.5 ppm, a triplet at 2.6 ppm and a double doublet at 3.6 ppm. It can be confidently hypothesized that the species in question is chloroethyl ethylsulfoxide (CEESO). In fact the spectrum also shows a nearly optimal integral ratio (3:2:2:2) along with the expected peak multiplicity. In this regard, the presence of a double doublet at 3.6 ppm assigned to C*H*$_2$-Cl instead of a triplet, as observed in pure CEES and $CEESO_2$, can be explained by assuming that the oxidation of CEES generates a chiral sulfoxide that in turn makes the methylenic protons adjacent to CH_2Cl diastereotopic, hence not chemically equivalent.[35]

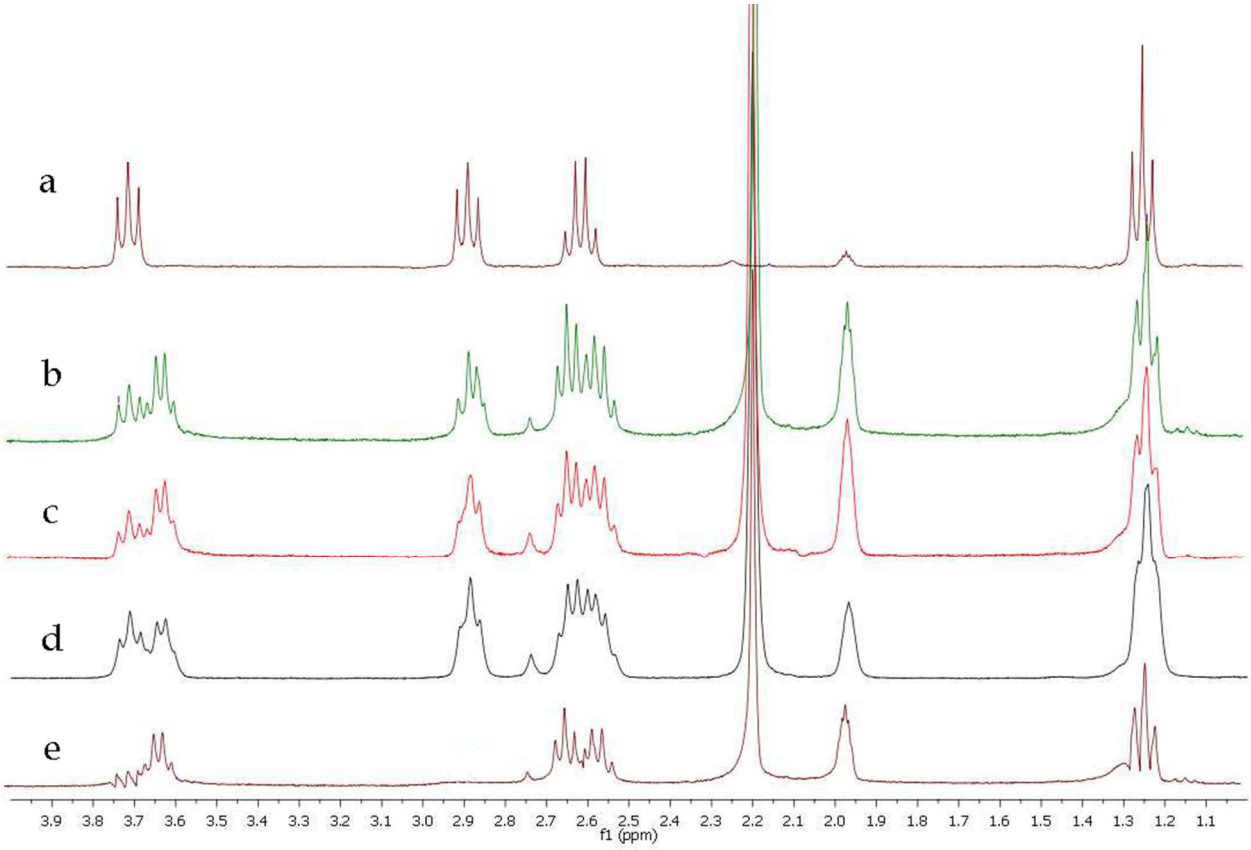

Figure 6. NMR spectra of CEES (a), FeOH-GO E (b), FeOH-GOU E (c), FeOH (d), and graphical spectral subtraction of *a* from *c* (d).

The NMR spectra of the extracts from the exhausted composites do not differ between each other in terms of the nature of the compounds found (i.e., CEES, CEESO and EVS). However, the comparison of the peak areas allows for a direct quantification of CEESO. When in contact with FeOH-GO and FeOH-GOU its yield turned out to be 14.1% and 14.5% higher, respectively, than that for FeOH only. This is a clear indication of the superior oxidizing properties of the graphite oxide-containing composite.

In order to determine the molecules whose concentration was beyond the detection limit of the NMR, the extracts were analyzed by tandem mass spectrometry using the enhanced product ion

(EPI) mode. The identification of the compounds with the EPI is summarized in Table 2. The mass spectra are included in Supplementary Information (Figures S2-S4).

The collected information suggests that several reactions occur on the solid/vapor interface of the materials. The CEES elimination pathway starts with its adsorption on the surface. The TA-MS suggested two adsorption centers of various energies for both, CEES and EVS. The first adsorption center implies a weak physical adsorption that can be simply due to the deposition of the volatilized molecules and/or polar interactions with the Lewis sites,[8] as represented in reaction 1.

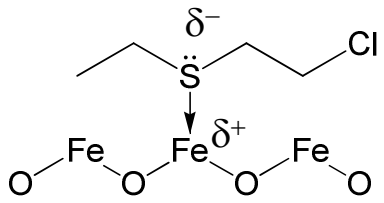

(Reaction 1)

These polar interactions are relatively weak leading to the desorption of adsorbed molecules at low temperatures.

Another adsorption site represents the strong adsorption of CEES. It has been reported that the CEES molecule has the ability to form hydrogen bonds (both S and Cl moieties) with the surface of metal oxides.[6] The attachment of the CEES molecules might occur mainly by hydrogen bonding to the OH groups (Reaction 2), Therefore, the enhancement in the CEES uptake by the GO and GOU presence is due to the increase in the number of OH groups in the composite.[20]

Table 2. Compounds detected (EPI-MS) and their representative mass-to-charge (m/z) fragments.

Sample name	Compounds detected*	m/z fragments and normalized abundance in parenthesis
FeOH E	CEES	125 (100), 110(23.6), 76(31.5)
	EVS	89(51.0), 61(31.0), 60(100)
	EVSO	105(23.0), 87(62.0), 85(62.0), 77(4.0), 61(96.0), 60(27.0), 59(100)
	2-butanol	75(26.8), 60(45.9), 59(100), 58(52.0)
	CAA	78(68.0), 77(4.6), 76(16.8), 75(100), 61(6.0)
	$CEESO_2$	157(73.4), 141(36.8), 122(11.7), 97(37.0), 95(37.0), 63(100)
	HEES	107 (12.5), 106(76.7), 91(42.9), 79(100), 77(29.4)
FeOH-GOE	CEES	125 (100), 110(2.1), 76(6.6)
	EVS	89(17.6), 61(100), 60(29)
	$HEESO_2$	123(100), 108(60.5), 107(73.7), 93(21.0), 79(46), 78(27.6)
	2-butanol	75(100), 60(17.3), 59(63.3), 58(26.9)
	EVSO	105(20.1), 87(3.4), 85(3.6), 77(19.4), 61(2.5), 60(31.3), 59(100)
	CEESO	141(20.9), 127(100), 113(8.13), 97(9.3), 63(90.7)
	BHetCl	281(57.8), 264(35.3), 246(52.4), 240(100), 208(6.8), 204(8.8), 198(20.4), 191(14.7), 169(10.6), 153(12.2)
	$CEES_2$	157(47.4), 129(9.8), 96(9.8), 95(7.0), 94(5.2), 63(100), 61(10.5)
FeOH-GOU E	CEES	125(100), 110(27.2), 76(49.5)
	EVS	89(43.2), 61(100), 60(30.9)
	2-butanol	75(89.7), 60(33.6), 59(100), 58(44.8)
	EVSO	105(12.8), 87(6.1), 85(2.8), 77(33.6), 61(9.4), 60(100), 59(33.0)
	$CEESO_2$	157(28.5), 141(65.7), 122(9.2), 113(17.8), 97(17.0), 95(100), 63(10.7)
	HEESO	123(30.5), 108(6.2), 107(4.1), 93(8.0), 79(83.3), 78(100)
	CEESO	141(53.6), 127(53.5), 113(10.3), 97(14.1), 63(100)
	BHetCl	281(60.0), 264(46.9), 246(53.8), 240(100), 208(9.2), 204(10.7), 198(23.0), 19117.7), 169(18.5), 153(16.9)
	$CEES_2$	157(28.5), 129(14.3), 96(12.1), 95(100), 94(22.8), 61(12.8)

* *Abbreviations*: CEES- 2-chloroethyl ethyl sulfide, EVS- ethyl vinyl sulfide (EVS), EVSO- ethyl vinyl sulfoxide, CAA- Chloroacetaldehyde,$CEESO_2$ - 2-chloroethyl ethyl sulfone, HEES- 2-hydroxyethyl ethyl sulfide, HEESO- hydroxyethyl ethyl sulfoxide, CEESO- 2-chloroethyl ethyl sulfoxide, $CEES_2$-2-chloroethyl ethyl disulfide, BHetCl- Hydroxyethyl)-2-(2-Chloroethylthio) ethylsulphonium chloride..

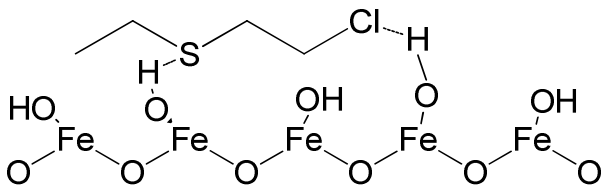

(Reaction 2)

The degradation of CEES into several compounds occurs after its initial adsorption. It has been reported that CEES can form a transient sulfonium cation as a result of the nucleophilic attack of sulfide onto the electrophilic carbon adjacent to Cl.[1] The sulfonium ion is very unstable and in the presence of water it hydrolyzes to hydroxyethyl sulfide.[36] Upon the adsorption CEES molecules, the formed sulfonium cations can either react with hydroxyl groups on the surface yielding HEES or can re-arrange themselves to form ethyl vinyl sulfide (EVS). The Lewis acidic Fe(III) center can promote the cleavage of the labile C-Cl bond and the subsequent intramolecular cyclization (Reaction 3) The chlorine will remain on the surface of the materials leading to the formation of a Fe-Cl bond.(Reaction 3). On the MS thermal profile of the exhausted samples a strong signal of m/z 35 was detected (Cl^{35}, Figure S5 in Supplementary Information) at the temperature of $FeCl_3$ decomposition (310 ºC). The intensity of the peak is clearly higher in the spectra of the exhausted FeOH-GO and FeOH-GOU samples. This indicates a more $FeCl_3$ in the composites, which in turn is related to more EVS in the headspace and on the surface. When hydroxyethyl ethyl sulfide is on the surface of the materials its dehydration can also result in the EVS formation (reaction 3).

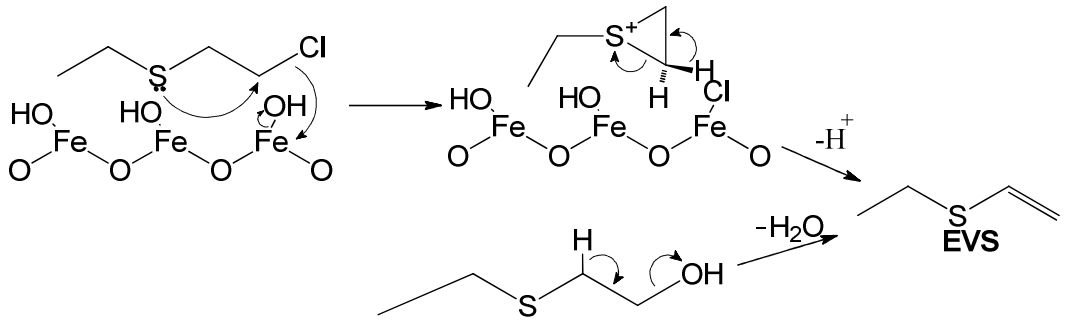

(Reaction 3)

The formation of EVS can be also photoassisted. Since in our previous study we reported that these materials can be photoactive in the visible range,[20] the following reaction is expected:

Surface of the material + $h\nu$ → Exited surface* (Reaction 4)

The absorption of a photon leads to the excitation of the adsorbent surfaces. When CEES interacts with the surface of the material(s), there is a photoinduced electron transfer which favors the formation of the ethyl ethyl sulfonium radical cation (EES+)[33, 37] (reaction 5):

$$Excited\ surface* + CEES \longrightarrow [Surface] - Cl^- + [EES]^+ \quad \text{(Reaction 5)}$$

The sulfonium cation forms EVS following the above-mentioned mechanism.

Ethyl vinyl sulfoxide (EVSO) was also detected on the surface of our samples. Its presence is due to the direct oxidation of the sulfide group by oxygen groups on the surface of the iron(III) oxide (Reaction 6), therefore reducing its surface. The reduction potential for Fe(III)+e^-→Fe(II) is 0.77 V,[38] which makes Fe(III)/Fe(II) couple a good oxidant pair. Furthermore, we recently reported the oxidation of sulfides by iron (hydr)oxide-based materials.[33]

In addition, the photocatalytic properties of the iron oxyhydroxide and the presence of atmospheric O_2 and H_2O on the surface of ferrihydrite[12] promotes the formation of hydroxyl and superoxide radicals (Reaction 6). These radicals have the potential to oxidize the adsorbed

sulfide molecules. The further oxidation of EVSO by the hydroxyl groups and/or radicals allows the formation of ethyl vinyl sulfone ($EVSO_2$). The hydroxyl/superoxide radicals can also promote the formation of HEES, CEESO, $CEESO_2$. HEES was formed in a significant amount on the surface of the samples, as evidenced by the broadening of the OH band in the FTIR spectra. The generation of thiyl radicals from HEES leads to a radical cation that can undergo a cleavage of the adjacent C-S bonds producing hydroxyalkyl and alkyl cations. The recombination of the (hydroxyl)alkyl cations can result in alcohols and in the detection of 2-butanol, as evidenced from the MS results.

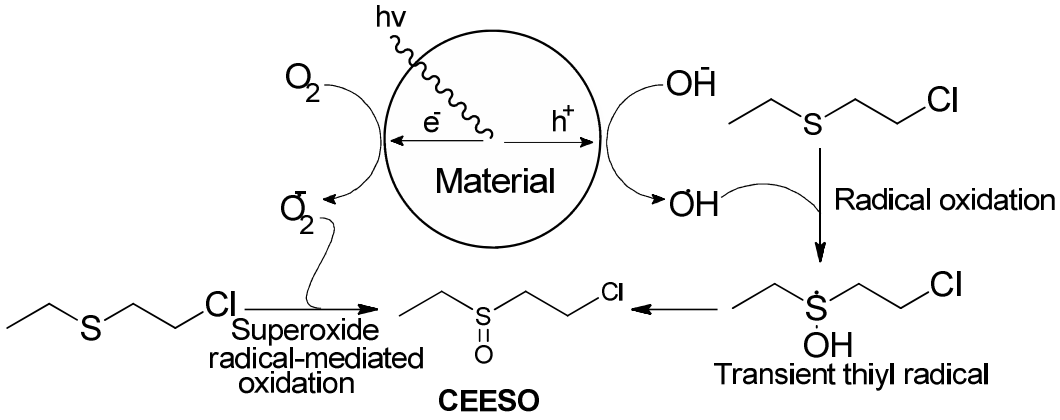

(Reaction 6)

On the surface of FeOH $CEESO_2$ was formed, and on the surfaces of the composites besides CEESO2 also CEESO was detected. The presence of these compounds indicates that sulfur oxidation took place before the chlorine was removed. Generally, more oxidized compounds were detected on the composites. This is owing to more hydroxyl groups than on the surface of FeOH and/or to the formation of hydroxyl/oxygen radicals.

Although the oxidized sulfur compounds were detected in the extract of FeOH, disulfides were identified on the composites only. It has been reported that the formation of disulfides is caused by the recombination of the thiyl radicals.[4] The two compounds detected were $CEES_2$ and

BHetCl, and their presence indicates that in the composites the activation and recombination of the thiyl radicals takes place. These disulfides of high molecular weight are responsible for the sulfur signals detected at high temperatures on the m/z profiles of the composites. Disulfides are still toxic compounds whose toxicity has discussed previously.[39, 40]

As we reported elsewhere,[20] the addition of graphite oxide into the ferrihydrite structure increases the surface area, the number of terminal groups, and also has an effect on the optoelectronic properties of the composites. All these physicochemical changes in the materials allowed the formation of the thiyl radicals from adsorbed molecules. Also, the higher concentration of sulfoxides quantified via NMR confirms the higher oxidative potential of the FeOH/GO and FeOH/GOU composites than that of iron oxyhydroxide.

As evidenced by UV-Vis-NIR, it is possible that Fe(III) d electrons are involved in CEES uptake. The sulfur atom in the CEES can complex the Fe(III) center by donating the lone electron pair, leading to the formation of the Fe-S coordination compound. In this study the presence of any Fe-S complex and/or iron sulfide or sulfate could not be confirmed. However, it cannot be discarded and it is possible that any of these compounds also contributed to the weight loss of the exhausted materials at high temperatures.

Experimental

Materials synthesis

The procedure for the synthesis of the reactive adsorbents used in this study was reported elsewhere.[20] Briefly, the iron oxyhydroxide (FeOH) was obtained by preparing 350 mL of a 0.026 M solution of $FeCl_3 \cdot 6H_2O$ and after, 660 mL of a 0.05 M solution of NaOH were slowly added under vigorous stirring. After the red-brown precipitate was formed, it was rapidly

decanted, then rinsed several times with deionized water until no AgCl precipitate was present in the rinsing solution upon $AgNO_3$ addition. Finally, the FeOH sample was dried during 12 h at 100 ºC.

The procedure for the composites' preparation was similar to that followed for FeOH. Before the NaOH addition, graphite oxide (GO) obtained by the Hummers' method[41] or nitrogen modified graphite oxide (See [20] for preparation details, GOU) were mixed with the $FeCl_3 \cdot 6H_2O$ solution and sonicated for 1 h to promote a graphite oxide dispersion. After, 660 mL of 0.05 M NaOH were slowly added to the suspension. The precipitate was collected and rinsed until no chloride was detected and finally dried at 100 ºC for 12 h. Samples are referred to as FeOH-GO and FeOH-GOU, depending on the type of GO used.

Exposure to CEES vapors

The experimental setup for the exposure of the materials to the CEES vapors was reported previously.[20] A glass vial containing 150 mg of the sample was introduced into a 160 mL reaction vessel and 300 µL of CEES was injected through a septum into a 5 mL beaker in the reaction vessel. The containers were kept under visible light (Xenon lamp, Solar light Co., INC, XPS-150^{TM}; less than 8% of the radiation is UV < 290 nm; the irradiance: 21.2 W/cm^2) at room temperature for 24 h. After the time was reached, vapor phases from the headspace of the containers were sampled with a syringe and injected into a GC-MS. Immediately after sampling, the exhausted materials were removed from the reaction vessels and stored in dark containers at -18 °C.

FTIR-ATR

The analyses were carried out on a Nicolet Magna-IR 380 spectrometer, by using the Smart MIRacle accessory that measures the attenuated total reflectance (ATR). The spectrum was collected 64 times and corrected for background noise. Experiments were done without KBr addition.

Gas Chromatography-Mass spectrometry (GC-MS)

The volatile reaction products were analyzed by using a GCMS-QP5050A (Shimadzu). The separation of the compounds was performed in a XTI-5 column (5% dephenyl-95% dimethyl polysiloxane) of 30 m length, 0.25 mm internal diameter, and 0.25 μm of liquid film thickness. The GC operation program was as follows: an increase from 50 ^{o}C to 100 ^{o}C at a rate of 5 deg min^{-1}, then the rate was changed to 40 deg min^{-1} up to 280 ^{o}C. Helium was used as a carrier gas. The injection volume, total flow and, the split ratio were 40 μL, 17.8 mL and 8, respectively. The mass spectrometer detector was used in an electron impact ionization mode.

Extraction protocol

In order to qualitatively determine the CEES reactive adsorption products that were deposited on the surface of the materials, an extraction with acetonitrile was carried out. The procedure for the solid-liquid extraction was as follows: 50 ± 2 mg of exhausted material was equilibrated with 1 mL of solvent during 5 days. The equilibration was carried out in the absence of light and a temperature of 30 °C under constant stirring. After, the extract was filtered and the liquid was stored at -18 °C.

Nuclear magnetic resonance spectrometry

Solid-liquid extractions with deuterated acetonitrile (CD_3CN) were carried out in the same conditions as outlined above with the exception of scaling down the amounts to require only 1 ml CD_3CN per extraction. 1H-NMR spectra were acquired on a Varian (300 MHz) at room temperature and peaks were assigned both by recording NMR spectra of standard compounds when commercially available, i.e. CEES, EVS and $EVSO_2$ and via comparison with literature data.

Mass Spectrometer-based analysis

Each extract was filtrated and subsequently injected into a mass spectrometry system (Q-TRAP 400, Applied Biosystems). The two modes used were: Enhanced Product Ion (EPI) ion spray voltage of 5500 V (highest sensibility), collision energy from 10-50 V (depending on the molecular weight selected), collision energy spread of 40 V, and a declustering potential of 80 V. Nitrogen gas was used as a curtain and collision gas. The identification of the compounds was made by analysis of the fragmentation of the parent molecules in positive ionization mode.

Simultaneous Thermal Analysis-Mass Spectroscopy (TA-MS)

Thermogravimetric (TG), derivative thermogravimetric (DTG), and simultaneous Thermal Analysis-Mass Spectroscopy (TA-MS) analyses were obtained in a SDT 2960 from TA instruments. The samples were heated at a rampage of 10 ºC min^{-1} from room temperature up to 1000 ºC. A flow of 100 mL min^{-1} of He (ultra-dry) was maintained during the analyses. The released products from the surface of the adsorbents were identified by a ThermoStar Gas Mass Spectrometer (GSD; Pfeiffer Vacuum) connected to the thermal analyzer. The off-gas collected was scanned with a Secondary Electron Multiplier (SEM) detector and a Faraday detector. The

m/z identified in the MS were correlated in real time with their corresponding temperatures in the thermal analysis.

Ultraviolet-visible-near infrared (UV-Vis-NIR) spectroscopy.

The spectra were obtained in a Cary500 Scan spectrometer (Varian) by using the Cary 500 diffuse reflectance accessory (integrated sphere). Before the analyses, the samples were compressed to form 0.65 mm thick pellets. The samples were mounted on a black tape and fitted into an integration sphere analysis port. The integration sphere was operated to collect diffuse reflection.

Conclusions

The results presented herein indicate that the adsorption of CEES on FeOH, FeOH-GO, and FeOH-GOU leads to its degradation into several compounds, whose majority remains adsorbed on the surface. The main reaction product of the CEES adsorption is EVS, which also was the only reaction product detected in the headspace of the reaction vessels. Besides being released, EVS was also retained on the surface. Two adsorption sites of various energies for both CEES and EVS are identified. They are linked to polar interactions with the Lewis site (weak) and hydrogen bonds with terminal hydroxyl groups (strong). Several oxidation compounds such as, CEESO, HEES, EVSO, CEESO, $CESSO_2$ were found on the surface of the materials. It is proposed that the high density of oxygen groups enhanced by the presence of GO and GOU promotes the oxidation of CEES and further oxidation of EVS adsorbed molecules. The photoassisted formation of hydroxyl and oxygen radicals also contributes to this oxidation. The presence of CEESO and $CEESO_2$ is an indicative that sulfur oxidation occurs before the chlorine

has been removed. Graphite oxide and aminated graphite oxide in the composite with ferrihydrite promote the production of sulfur radicals on the materials' surface. 2-butanol and disulfides are the result of the cleavage and recombination of thiyl radicals.

Acknowledgements

This study was supported by the ARO (Army Research Office) grant W911NF-13-1-0225 and NSF collaborative SBET Grant no.1133112.

References

1 A. Roy, A. K. Srivastava, B. Singh, T. H. Mahato, D. Shah and A. K. Halve, *Microporous Mesoporous Mater.*, 2012, **162**, 207-212.

2 L. Bromberg, N. Pomerantz, H. Schreuder-Gibson and T. A. Hatton, *Ind. Eng. Chem. Res.*, 2014, **53**, 18761-18774.

3 C. W. Kanyi, D. C. Doetschman and J. T. Schulte, *Microporous Mesoporous Mater.*, 2009, **124**, 232-235.

4 A. V. Vorontsov, C. Lion, E. N. Savinov and P. G. Smirniotis, *J. Catal.*, 2003, **220**, 414-423.

5 I. N. Martyanov and K. J. Klabunde, *Environ. Sci. Technol.*, 2003, **37**, 3448-3453.

6 D. Panayotov and J. T. Yates, *J. Phys. Chem. B*, 2003, **107**, 10560-10564.

7 S. Dadvar, H. Tavanai, M. Morshed and M. Ghiaci, *J. Chem. Eng. Data*, 2012, **57**, 1456-1462.

8 D. B. Mawhinney, J. A. Rossin, K. Gerhart and J. T. Yates, *Langmuir*, 1999, **15**, 4789-4795.

9 B. Singh, T. H. Mahato, A. K. Srivastava, G. K. Prasad, K. Ganesan, R. Vijayaraghavan and R. Jain, *J. Hazard. Mater.*, 2011, **190**, 1053-1057.

10 N. M. Okun, T. M. Anderson and C. L. Hill, *J. Mol. Catal. A: Chem.*, 2003, **197**, 283-290.

11 R. M. Narske, K. J. Klabunde and S. Fultz, *Langmuir*, 2002, **18**, 4819-4825.

12 R. M. Cornell and U. Schwetmann, *The Iron Oxides Structure, Propeties, Reactions, Ocurrences and Uses*, Wiley-vch, Winheim, Germany, 2 edn., 2004.

13 D. M. Sherman, *Geochim. Cosmochim. Acta*, 2005, **69**, 3249-3255.

14 G. Liu, S. Liao, D. Zhu, L. Liu, D. Cheng and H. Zhou, *Mater. Res. Bull.*, 2011, **46**, 1290-1295.

15 B. Gilbert, C. Frandsen, E. R. Maxey and D. M. Sherman, *Phys. Rev. B*, 2009, **79**, 035108.

16 S. K. Park, T. Ishikawa and Y. Tokura, *Phys. Rev. B*, 1998, **58**, 3717-3720.

17 G. Liu, S. Debnath, K. W. Paul, W. Han, D. B. Hausner, H.-A. Hosein, F. M. Michel, J. B. Parise, D. L. Sparks and D. R. Strongin, *Langmuir*, 2006, **22**, 9313-9321.

18 V. Štengl, V. Houšková, S. Bakardjieva, N. Murafa, M. Maříková, F. Opluštil and T. Němec, *Mater. Charact.*, 2010, **61**, 1080-1088.

19 V. Štengl, T. M. Grygar, F. Opluštil and T. Němec, *J. Hazard. Mater.*, 2011, **192**, 1491-1504.

20 J. A. Arcibar-Orozco and T. J. Bandosz, *J. Mater. Chem. A*, 2015, **3**, 220-231.

21 K. Rout, M. Mohapatra and S. Anand, *Dalton Trans.*, 2012, **41**, 3302-3312.

22 G. Socrates, *Infrared and Raman Characteristic Group Frequencies: Tables and Charts*, Wiley, West Sussex, England, 2004.

23 R. Davis, M. Frearson and F. E. Prichard, *Mass spectrometry*, Wiley, London, England, 1987.

24 E. Pretsch, P. Bühlmann and C. Affolter, *Structure Determination of Organic Compounds: Tables of Spectral Data*, Springer-Verlag Berlin Heidelberg, Berlin, Germany, 3 edn., 2000.

25 R. C. Weast and J. G. Grasselli, *Handbook of Data on Organic Compounds*, CRC Press, Boca Ratton, US, 1989.

26 R. J. Fruehan, *Metall. Trans. B*, 1977, **8**, 279-286.

27 C. Petit, M. Seredych and T. J. Bandosz, *J. Mater. Chem.*, 2009, **19**, 9176-9185.

28 J. A. Arcibar-Orozco, J. R. Rangel-Mendez and T. J. Bandosz, *J. Hazard. Mater.*, 2013, **246–247**, 300-309.

29 Y. Zhao, M. Seredych, Q. Zhong and T. J. Bandosz, *RSC Advances*, 2013, **3**, 9932-9941.

30 A. C. Scheinost, A. Chavernas, V. Barron and J. Torrent, *Clays Clay Miner.*, 1998, **46**, 528-536.

31 H. Zhang, X. Lv, Y. Li, Y. Wang and J. Li, *ACS Nano*, 2010, **4**, 380-386.

32 J. Torrent and V. Barrón, Diffuse reflectance spectroscopy of iron oxides, in *Encyclopedia of Surface and Colloid Science*, CRC press, Boca Raton, US, 2002, pp. 1438-1446.

33 D. A. Giannakoudakis, J. A. Arcibar-Orozco and T. J. Bandosz, *Appl. Catal. B-Environ.*, 2015, **174–175**, 96-104.

34 H. Tang, X. Zhou, Y. Guan, L. Zhou, X. Wang and H. Yan, *Ecotoxicol. Environ. Saf.*, 2013, **91**, 46-51.

35 R. M. Silverstein, F. X. Webster and D. Kiemle, *Spectrometric Identification of Organic Compounds, 7th Edition*, Wiley, New Jersey, US, 7 edn., 2005.

36 Y. C. Yang, L. L. Szafraniec, W. T. Beaudry and J. R. Ward, *J. Org. Chem.*, 1988, **53**, 3293-3297.

37 T. H. Mahato, G. K. Prasad, B. Singh, K. Batra and K. Ganesan, *Microporous Mesoporous Mater.*, 2010, **132**, 15-21.

38 M. B. Mitchell, V. N. Sheinker and E. A. Mintz, *J. Phys. Chem. B*, 1997, **101**, 11192-11203.

39 R. O. Beauchamp, Jr., J. S. Bus, J. A. Popp, C. J. Boreiko and L. Goldberg, *Crit Rev Toxicol*, 1983, **11**, 169-278.

40 R. W. Wood, *Neurotoxicol. Teratol.*, 1981, **3**, 397-405.

41 W. S. Hummers and R. E. Offeman, *J. Am. Chem. Soc.*, 1958, **80**, 1339-1339.